ACS APPLIED MATERIALS & INTERFACES

Research Article

www.acsami.org

Tunable Plasticity in Amorphous Silicon Carbide Films

Yusuke Matsuda,[†] Namjun Kim,[‡] Sean W. King,[§] Jeff Bielefeld,[§] Jonathan F. Stebbins,[‡] and Reinhold H. Dauskardt*[,†,⊥]

[†]Department of Materials Science and Engineering, Stanford University, Stanford, California 94305, United States

[‡]Department of Geological & Environmental Sciences, Stanford University, Stanford, California 94305, United States

[§]Logic Technology Development, Intel Corporation, Hillsboro, Oregon 97124, United States

ABSTRACT: Plasticity plays a crucial role in the mechanical behavior of engineering materials. For instance, energy dissipation during plastic deformation is vital to the sufficient fracture resistance of engineering materials. Thus, the lack of plasticity in brittle hybrid organic–inorganic glasses (hybrid glasses) often results in a low fracture resistance and has been a significant challenge for their integration and applications. Here, we demonstrate that hydrogenated amorphous silicon carbide films, a class of hybrid glasses, can exhibit a plasticity that is even tunable by controlling their molecular structure and thereby leads to an increased and adjustable fracture resistance in the films. We decouple the plasticity contribution from the fracture resistance of the films by estimating the "work-of-fracture" using a mean-field approach, which provides some insight into a potential connection between the onset of plasticity in the films and the well-known rigidity percolation threshold.

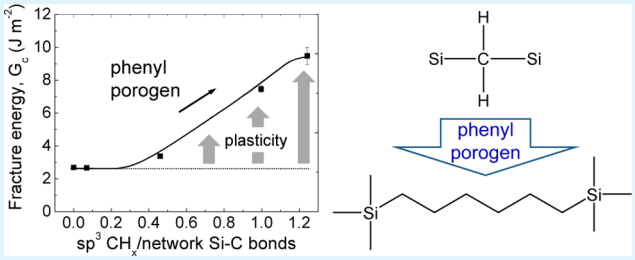

KEYWORDS: *hybrid materials, structure–property relationship, mechanical properties, thin films, rigidity percolation, chemical vapor deposition*

1. INTRODUCTION

Plasticity plays a crucial role in the mechanical behavior of engineering materials. For instance, cohesive fracture resistance, G_c, is the sum of the "work-of-fracture," G_o, needed to rupture atomic bonds at the crack tip and energy dissipation through plastic deformation, G_{pl}, during bond rupture processes. G_{pl} is usually far greater than G_o and therefore the lack of plasticity in brittle materials often results in a low G_c. This lack of plasticity has particularly been a serious issue for brittle hybrid organic–inorganic glasses (hybrid glasses) because their glass network connectivity is reduced by the presence of monovalent bonds and/or additional nanoporosity,[1−5] which also reduces G_o. The poor mechanical properties of brittle hybrid glasses pose a significant challenge for their integration and application[1−5] and limit exploiting their excellent multifunctional properties.[1,6,7]

We have recently developed hydrogenated amorphous silicon carbide (a-SiC:H) films, a class of hybrid glasses, that exhibit plasticity leading to a markedly increased G_c in spite of the presence of nanoporosity (∼12 vol %).[8] The films had carbon-rich nonstoichiometric composition and presented excellent thermal and chemical stability (∼400 °C). However, the origin of the plasticity in the nonstoichiometric films has not been well understood. In particular, different nonstoichiometric films with similar chemical composition to those with plasticity did not exhibit any plasticity.[8]

Here, we demonstrate that the plasticity in the non-stoichiometric a-SiC:H films originates from the presence of sp^3 hybridized CH$_x$ chains, and plasticity contribution to the G_c of the films is tunable by finely controlling their molecular structure. We first characterize the molecular structure of the nonstoichiometric films using ^{13}C solid-state nuclear magnetic resonance (NMR) spectroscopy complemented by Fourier transform infrared (FTIR) spectroscopy and show that sp^3 CH$_x$ chains are incorporated into the glass network through the decomposition of phenyl porogen precursors (porogen) used to generate nanoporosity in the films. We then show that the number of sp^3 CH$_x$ chains is even controllable by varying the porogen content, which leads to a tunable plasticity and G_c of the nonstoichiometric films between 2.7 and 10.0 J m^{-2}. Finally, we attempt to decouple the plasticity contribution of the films from their G_c by estimating G_0 using a mean-field approach, which reveals a potential connection between the onset of plasticity and well-known rigidity percolation threshold.

2. EXPERIMENTAL SECTION

All of the a-SiC:H films were generated by plasma-enhanced chemical vapor deposition (PECVD). a-SiC:H films with widely varying compositions were deposited on a 300 mm diameter (100) silicon wafer using a manufacturing PECVD system at 250 and 400 °C, similar to methods described elsewhere.[9−11] Targeted film compositions were obtained by tuning the amount of precursors, including methylsilanes, phenylsilanes, He, and H_2. Depending on the Si and C ratio, the a-SiC:H films were classified into either nonstoichiometric films (C/Si > 1, SiC-1 through SiC-5 in Table 1) or stoichiometric

Received: May 28, 2013
Accepted: July 22, 2013
Published: July 22, 2013

Table 1. Material Properties of a-SiC:H Films[a]

film designation	density, ρ (g/cm^3)	Young's modulus, E (GPa)	hardness, H (GPa)	yield stress, σ_{ys} (MPa)	dielectric constant, k	porosity (vol %)	main precursors
SiC-1 (NS)	1.1	6.4	0.85	792 ± 43	3.2	2	$H_xSi(C_yH_z)_{4-x}$
SiC-2 (NS)	1.2	4.2	0.31	104 ± 11	2.8	12	$H_xSi(CH_3)_{4-x}$/porogen
SiC-3 (NS)	1.2	3.8	0.31	71 ± 13		13	$H_xSi(CH_3)_{4-x}$/porogen
SiC-4 (NS)	1.2	3.8	0.40	165 ± 30		10	$H_xSi(CH_3)_{4-x}$/porogen
SiC-5 (NS)	1.3	8.0	1.43	430 ± 45		5	$H_xSi(CH_3)_{4-x}$/porogen
SiC-6 (S)	1.6	25.7	4.50	995 ± 166		0	$H_xSi(CH_3)_{4-x}$
SiC-7 (S)	1.6	35.8	5.63		4.8	0	$H_xSi(CH_3)_{4-x}$
SiC-8 (S)	1.4	15.6	2.54		4.4	0	$H_xSi(CH_3)_{4-x}$
SiC-9 (S)	1.3	11.5	1.89		4	0	$H_xSi(CH_3)_{4-x}$
SiC-10 (S)	1.2	6.2	0.58		3.6	5	$H_xSi(CH_3)_{4-x}$
SiC-11 (S)	1.2	6	0.70		3.7	4	$H_xSi(CH_3)_{4-x}$

[a]S and NS in parentheses represent stoichiometric and non-stoichiometric composition, respectively. SiC-6 is the base film for SiC-2 through SiC-5.

(C/Si ~1, SiC-6 through SiC-11 in Table 1). One of the nonstoichiometric films with plasticity (SiC-2) was generated by modifying SiC-6 with additional phenyl-based porogens which is described in elsewhere.[12] The nonstoichiometric films were subsequently cured by e-beam irradiation at ~400 °C so as to remove the porogen precursors and to generate nanoporosity (12 vol %). Deposition time was adjusted to have nominal thickness of 500 nm, and the bottom and top sides of the a-SiC:H films were capped with 25 nm silicon carbon nitride (SiCN) layers, which were deposited by the same PECVD system.[9]

Material properties of a-SiC films were determined by various characterization techniques. Low frequency dielectric constants (at 100 kHz) of the films were measured using a Hg probe.[9] Film density was determined by X-ray reflectivity technique.[13] The Young's modulus of films was determined by nanoindentation[14] with Poisson's ratio of 0.25, using the film thickness of 2000 nm to minimize substrate effects. The yield stress of the nonstoichiometric films was measured by nanoindentation using the cavity model.[15] Film porosity was measured by spectroscopic ellipsometry with toluene solvent. These material properties are listed in Table 1.

To determine the hybridized bonding state of C atoms in the nonstoichiometric a-SiC:H films, ^{13}C and ^{29}Si magic angle spinning (MAS) nuclear magnetic resonance (NMR) spectroscopy was performed. Powder samples were prepared for NMR experiments by removing the a-SiC:H films from the silicon substrates with a razor blade; typically about 20−25 mg of samples were used. The spectra were collected using a Varian Infinity Plus 400 spectrometer (9.4 T) at 100.52 MHz for ^{13}C and 79.42 MHz for ^{29}Si. A 3.2 mm Varian/Chemagnetics T3MAS probe was used with spinning rates of 12 kHz. Spectra were collected with single pulse acquisition without cross-polarization, to ensure quantitative peak areas. For ^{13}C, a pulse length of 1.2 μs (45° RF tip angle) and a pulse delay of 60 s were used to ensure that measured relative peak intensities were not affected by differential relaxation. A spectrum was also collected with a 360 s pulse delay for one sample and no significant intensity increase was observed. Typically 3000−5000 acquisitions were accumulated to improve the signal-to-noise ratio. ^{29}Si MAS NMR spectra were collected for two samples (SiC-1, 2) with a pulse width of 1.0 μs (45° RF tip angle) and pulse delay of 10 s, and about 30 000 acquisitions were averaged for each spectrum. Chemical shifts are referenced to tetramethylsilane (TMS) at 0 ppm for both ^{13}C and ^{29}Si.

Molecular structure of the a-SiC:H films was also characterized by transmission mode Fourier transform infrared spectroscopy (FTIR, Nicolet Magna-IR 860 and Bio-Rad QS-3300 spectrometers) in the wavenumber range from 400 to 4000 cm^{-1}. Details on FTIR characterization of the a-SiC:H films are described elsewhere.[11] To determine glass network connectivity, the elemental composition of the a-SiC:H films were determined by combined nuclear reaction analysis (NRA) and Rutherford backscattering spectroscopy (RBS).[10]

The fracture energy, G_c, of a-SiC films was measured by double cantilever beam (DCB) testing with a Delaminator Test System (DTS, Menlo Park, CA). In sample preparation, a-SiC:H films were bonded to silicon wafers with epoxy adhesives (Figure 1), which were then

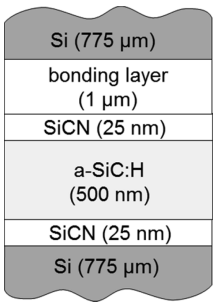

Figure 1. Schematic illustration of sandwiched multilayered thin film structures (not to scale).

diced by a high-speed wafer saw to fabricate DCB specimens, 5 mm wide, 1.56 mm in total thickness, and 50 mm in length. The DCB specimens were loaded in pure mode I, and displacement was measured to determine G_c in a laboratory environment at ~25 °C and ~40%RH. The test method for characterizing G_c is detailed elsewhere.[16,17] All mating fracture surfaces were characterized by XPS survey scan to identify the fracture paths as being either adhesive at the interface of the a-SiC:H film or cohesive in the film.

3. RESULTS AND DISCUSSIONS

3.1. Molecular Structure Characterization by Solid-State NMR and FTIR. The molecular structure of the carbon rich nonstoichiometric a-SiC:H films (SiC-1 and SiC-2) was characterized by ^{13}C solid-state NMR (Figure 2a). Note that SiC-2 is the film that exhibited plasticity in our previous study.[8] The ^{13}C NMR spectra show two main peaks at ~0 and ~135 ppm corresponding to sp^3 and sp^2 C atoms, respectively. The peak at ~0 ppm represents C atoms in C−Si bonds.[18] A striking difference between the SiC-1 and SiC-2 films is that there is an additional peak at ~20 ppm only in SiC-2, which corresponds to sp^3 CH_x chains that are not directly bonded with Si atoms.[18−20] These sp^3 CH_x chains can undergo plastic deformation through molecular relaxation processes as ductile polymers, which suggests that they are responsible for the plasticity in SiC-2. In addition, ^{29}Si solid-state NMR spectra for these two nonstoichiometric films did not exhibit any significant difference in their molecular structure (Figure 2b), corroborating the suggested mechanism for the plasticity. The broad ^{29}Si NMR peaks centered near 0 ppm are consistent with Si primarily with four carbon, or three carbon and one oxygen,

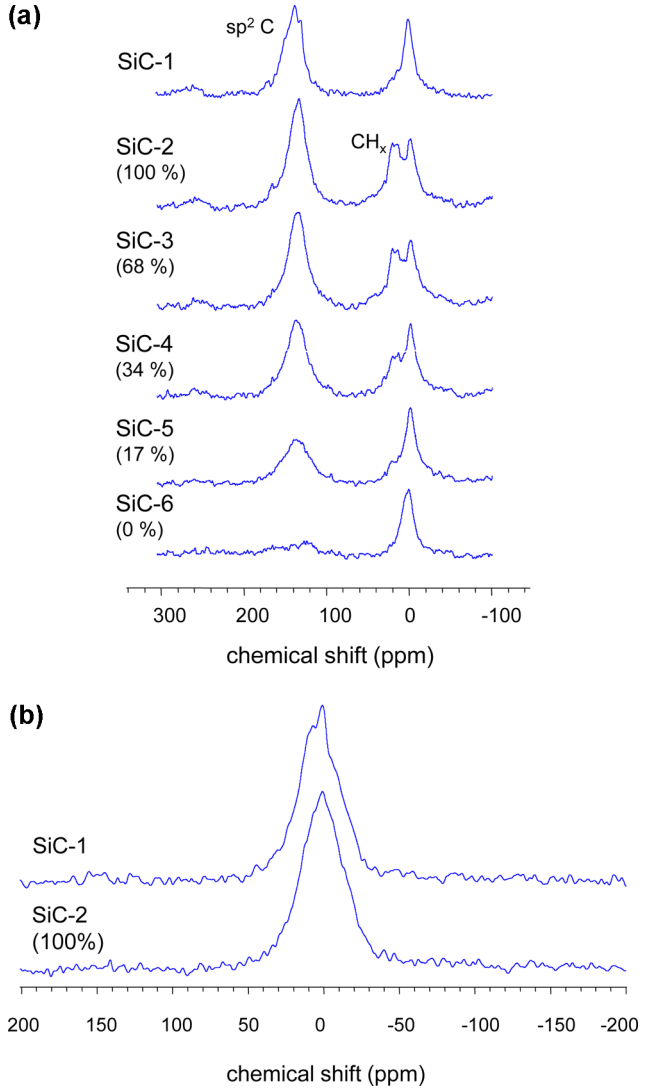

Figure 2. NMR spectra for selected a-SiC:H films: (a) ^{13}C; (b) ^{29}Si. Number in parentheses represents the amount of the porogen relative to SiC-2.

neighbors in a disordered structure, as indicated by the measured C/Si and O/Si ratios.[21] The shapes and widths of the peaks are very similar, indicating similar distributions of Si−C and/or Si−O linkages. Little or no signal appears in the region below about −30 ppm, where Si sites with multiple O neighbors are expected.

We believe that the origin of these sp^3 CH_x chains is the porogen, which was introduced in addition to the main precursors (methylsilane) during the PECVD process in order to generate nanoporosity in SiC-2. This proposition is supported by ^{13}C NMR spectrum for SiC-6, which was generated under the same deposition condition for SiC-2 except that no porogen precursor was used. The peak for the sp_3 CH_x chains at ∼20 ppm was not observed in the NMR spectrum for SiC-6. Furthermore, we generated films (SiC-3 through SiC-5) by varying the amount of the porogen relative to SiC-2 and collected the ^{13}C NMR spectra for these films. The intensity of the peak for the sp^3 CH_x chains increased with increasing amount of the porogen. sp^3 CH_x chains were not present in the molecular structure of the porogen, which thereby suggests that they formed through the decomposition of the porogen most likely during the e-beam irradiation at 400 °C. This formation of the sp^3 CH_x chains was completely unexpected because the porogen was designed to be removed during the irradiation.

FTIR characterizations for the films in the wavenumber range from 2700 to 3200 cm^{-1} (Figure 3) were consistent with

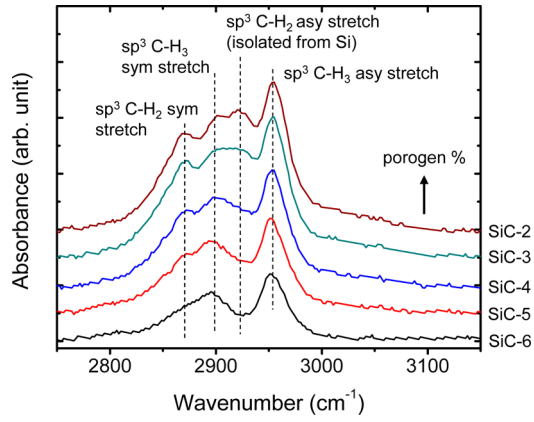

Figure 3. FTIR spectrum of C−H_x stretch for selected a-SiC:H films.

the NMR characterizations. A peak corresponding to sp^3 C−H_2 asymmetric stretch $(CH_x)_n$ chains isolated from Si[22,23] at ∼2930 cm^{-1} was observed only in the nonstoichiometric films with the porogen (SiC-2 through SiC-5). This peak intensity and another peak corresponding to sp^3 C−H_2 symmetric stretch modes both increased with increasing amount of the porogen, which indicates that some of the sp^3 CH_x groups should be sp^3 C chains.

3.2. Tunable Plasticity and Cohesive G_c. We examine how varying number of sp^3 chains influences the plasticity and resulting G_c of the films. The yield strength, σ_{ys}, of the nonstoichiometric a-SiC:H films (SiC-2 through SiC-6) as a function of relative porogen amount with respect to SiC-2 were measured by nanoindentation (▲ in Figure 4). The σ_{ys} of the

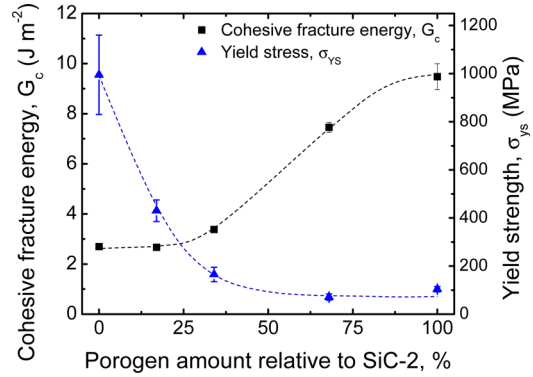

Figure 4. Yield strength and cohesive fracture energy of a-SiC:H films as a function of the amount of porogen relative to SiC-2.

films decreased with increasing porogen amount from 995 to 71 MPa. The cohesive G_c of these films increased from 2.7 to 10 J m^{-2} with increasing amount of porogen precursors (■ in Figure 4). To the best of our knowledge, this is for the first time that tunable plasticity was conferred to a-SiC:H films, which resulted in varying G_c.

3.3. Plasticity Contribution and Rigidity Percolation Threshold. We estimate the plasticity contribution to the

fracture resistance of the nonstoichiometric films by partitioning G_c into G_{pl} and G_0. In general, the estimation of G_{pl} is not simple because it usually requires computational analyses together with assumptions about a stress-separation function during bond rupture that determines G_0.[17,24,25] Instead, we employ a simple and phenomenological approach that is predicated on the scaling behavior between G_0 and the glass network connectivity for brittle fracture. Specifically, we estimate G_0 using a mean-field approach, which provides some insight into a connection between the onset of plasticity and the rigidity percolation threshold in topological constraint theory.[26−31]

In brittle materials like stoichiometric a-SiC:H films, $G_c \approx G_0$ and empirically expressed by[31]

$$G_o = \sum_i N_i \varepsilon_i \quad (1)$$

where the subscript i represents the bond type, N the ruptured bond density (bond m^{-2}) that is related to glass network connectivity, and ε the energy required to rupture bond (J $bond^{-1}$). ε is assumed to be comparable among the different stoichiometric a-SiC:H films because their network bonds are identical and have similar bond energy.[23,32,33] Accordingly, the G_0 of the brittle stoichiometric a-SiC:H films should primarily be governed by N. An accurate characterization of N for the a-SiC:H films is very difficult because of the absence of long-range order and their complex molecular structure, so we instead characterize an alternative measure that represents the glass network connectivity using a mean-field approach. This measure is characterized by counting the number of network bonds per atoms in the molecular structure and is hereafter referred to as average network bond number, $\langle r \rangle$, which is expressed by[26,27]

$$\langle r \rangle = \frac{\sum_i x_i n_i - 2x_H}{1 - x_H} \quad (2)$$

where the subscript i represents each different element, x the atomic fraction of the element, and n the number of bonds to each atom of the element (i.e., $n_{Si} = 4$, and $n_H = 1$). The first term in the numerator represents average bond number per atom including terminal bonds. The terms with x_H exclude H atoms from the glass network because they do not form any network bond.

To characterize the values of $\langle r \rangle$, x_i was determined by combined NRA and RBS together with ^{13}C NMR (Table 2). The ^{13}C NMR data (Figure 2a) was used to differentiate hybridization of C atoms in the nonstoichiometric films. Although C atoms preferably form sp^3 hybridized bonds with Si in stoichiometric compositions, the excess C atoms in the nonstoichiometric film can form both sp^2 (3-fold) and sp^3 (4-fold) bonds.[23,32,34] The ratio of sp^2 to sp^3 C atoms was determined by that of the area under the peaks corresponding to the two configurations. In addition, O atoms can form both monovalent bonds (OH) and network bridging bonds (Si−O−Si). Although it is possible to detect these OH and Si−O−Si bonds by FTIR, it is very difficult to differentiate them in our a-SiC:H films because of an overlapping interference between Si-CH_2−Si wagging mode and Si−O−Si stretching mode at ∼1000−1050 cm^{-1}.[8,23,35] Therefore, we considered two limits, in which all O atoms form either OH bonds or Si−O−Si bonds, to calculate $\langle r \rangle$. The characterized $\langle r \rangle$ listed in Table 2 was the average of the two limits. We note that the presence of O in the a-SiC:H Films is due primarily to water molecule diffusion into the films and subsequent hydration and condensation reactions that occurred after film deposition as described elsewhere.[8,32]

Table 2. Chemical Composition, sp^2/sp^3 C Ratio from Solid-State ^{13}C NMR, and Calculated Average Coordination Number for a-SiC:H Films[a]

film designation	NRA/RBS composition at % (± 5%) C	Si	O	H	NMR sp^2/sp^3 C ratio	avg network bond number $\langle r \rangle$
SiC-1 (NS)	30.2	10.6	9.6	49.6	1.49	2.31 ± 0.03
SiC-2 (NS)	38.6	5.0	4.3	52.2	1.33	2.29 ± 0.06
SiC-3 (NS)	40.9	6.3	2.3	50.5	1.09	2.47 ± 0.02
SiC-4 (NS)	39.5	8.0	3.1	49.5	1.09	2.51 ± 0.02
SiC-5 (NS)	33.6	11.2	3.3	51.9	1.12	2.47 ± 0.01
SiC-6 (S)	23.9	19.6	7.0	49.5	<0.10	2.75 ± 0.01
SiC-7 (S)	28.5	22.2	4.1	45.3		3.06 ± 0.04
SiC-8 (S)	24.0	20.5	5.9	49.7		2.83 ± 0.05
SiC-9 (S)	23.1	21.5	9.2	46.1		2.88 ± 0.08
SiC-10 (S)	21.9	16.6	8.2	53.2		2.56 ± 0.05
SiC-11 (S)	14.8	14.8	12.6	57.8		2.04 ± 0.01

[a]S and NS in parentheses represent stoichiometric and non-stoichiometric film composition, respectively. SiC-6 is the base film for SiC-2 through SiC-5.

Figure 5 shows the scaling between the quantified $\langle r \rangle$ and G_0 of the brittle stoichiometric films. The values of G_0 were taken

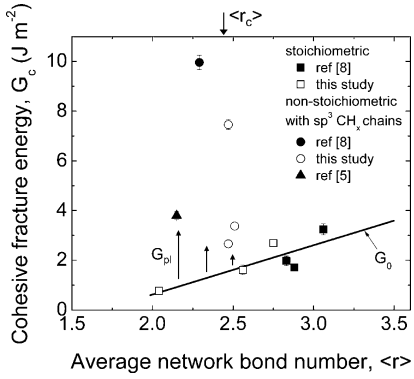

Figure 5. Cohesive fracture energy of a-SiC:H films as a function of average network bond number. $\langle r_c \rangle$ represents rigidity percolation threshold.

from the previous study[8] (■) as well as measured in this study (□). The G_0 of the stoichiometric films decreased with decreasing $\langle r \rangle$, which is consistent with eq 1 and demonstrates the important role of the glass network connectivity in brittle fracture similar to previous studies on organosilicate hybrid glasses.[4,36,37] The scaling was best fitted with a linear function $G_0 = 2.04\langle r \rangle - 3.48$. Now for the nonstoichiometric a-SiC:H films with plasticity, $G_c = G_0 + G_{pl}$, which are also plotted as a function of $\langle r \rangle$ in Figure 5 (● for SiC-2,[8] ○ for SiC-3 through SiC-5). Unlike the stoichiometric films, the nonstoichiometric films did not follow the linear scaling. The values of G_c for the nonstoichiometric films deviated from the linear scaling, and the extent of the deviation increased with decreasing $\langle r \rangle$. The types of network bonds in the stoichiometric and non-stoichiometric films are identical (Si−C, C−C, and Si−Si) and have comparable bond dissociation energies,[23,32,33] and

dx.doi.org/10.1021/am402046e | ACS Appl. Mater. Interfaces 2013, 5, 7950−7955

therefore the amount of the deviation from the linear scaling is interpreted as G_{pl}.

These analyses indicate that the onset of the plasticity contribution occurs when $\langle r \rangle$ falls below ~2.47, which almost coincides with the rigidity percolation threshold, $\langle r_c \rangle$, in topological constraint theory.[26−31] Although $\langle r_c \rangle \approx 2.4$ for most glasses, it should be increased for our nonstoichiometric films due to the presence of π bonds in their glass network. These π bonds restrict the rotation of the C atoms and provide 1/2 additional constraint to the glass network,[38] thereby increasing the $\langle r_c \rangle$ of the nonstoichiometric films as follows

$$\langle r_c \rangle = 2.4 + 0.2x_{C_{sp^2}} \quad (3)$$

where $x_{C_{sp}}{}^2$ is the atomic fraction of sp^2 C atoms in the films. Equation 3 can easily be obtained by counting additional 1/2 constraint per sp^2 C atoms. Using the values for $x_{C_{sp2}}$ listed in Table 2, the values of $\langle r_c \rangle$ for our nonstoichiometric were calculated ~2.44. Below the threshold, the glass network is underconstrained and flexible (so-called "floppy"),[26−31] which implies that there exists a potential connection between the onset of plasticity contribution and the rigidity percolation threshold.[37]

This is consistent with another study. We plot the value of G_c for recently reported cross-linked polycarbosilane (CLPCS) films, which consist of sp^3 C chains, Si−C bonds, and monovalent bonds,[5] similar to the nonstoichiometric films with plasticity and have $\langle r \rangle \approx 2.15$ well below the rigidity percolation threshold (▲ in Figure 5). The value of G_c for the CLPCS films is 3.8 J m^{-2}, much higher than that of the stoichiometric a-SiC:H films with the similar value of $\langle r \rangle$. Additionally, we note that transition of brittle hydrogenated amorphous carbon to polymeric hydrocarbon occurs at the rigidity percolation threshold.[39,40] We note that little plasticity observed in one of the stoichiometric films (SiC-11) at $\langle r \rangle$ much lower than $\langle r_c \rangle$ is related to the inherent lack of plasticity in Si−C−Si bonds. An implication of this study is that a combination of molecular structure leading to plasticity (i.e., sp^3 CH_x bonds) and the values of $\langle r \rangle$ below rigidity percolation threshold is necessary to observe the onset of plasticity in a-SiC:H films.

It is of significant interest in future studies to more systematically investigate whether there is indeed a fundamental connection between the onset of plasticity contribution and the rigidity percolation threshold for a-SiC:H films with sp^3 CH_x chains. The maximum value of $\langle r \rangle$ in a-SiC:H films is four, which is inherently reduced by imparting sp^3 CH_x chains into their glass network. In our study, it was not possible to generate a-SiC:H films with sp^3 CH_x chains that have a value of $\langle r \rangle$ greater than the rigidity percolation threshold. Another synthesis route[5] that can better control the number of sp^3 CH_x chains and their length in a-SiC:H films will be taken for our future studies.

CONCLUSIONS

We have demonstrated tunable plasticity in a-SiC:H films by controlling the molecular structure, which leads to the increased and tailored fracture resistance of the films. We decoupled the plasticity contribution to fracture resistance of the nonstoichiometric films by estimating the work-of-fracture using a mean field approach. We discussed a potential connection between the onset of the plasticity contribution and rigidity percolation threshold in topological constraint theory, which suggests that a underconstrained glass network having molecular element that can lead to plasticity (i.e., sp^3 CH_x bonds) is needed to observe plasticity contribution in a-SiC:H films. Tunable plasticity through second organic phases has a greater implication for toughening other hybrid glasses to enable their integration and application.

AUTHOR INFORMATION

Corresponding Author

*E-mail: dauskardt@stanford.edu. Tel/Fax: +1 (650) 725-0679/+1 (650) 725-4034.

Present Address

⊥Author R.H.D. is currently at 496 Lomita Mall, Durand Building, Room 121, Stanford University, Stanford, CA 94305

Notes

The authors declare no competing financial interest.

ACKNOWLEDGMENTS

This work was generously supported by the US Department of Energy under Contract DE-FG02-07ER46391. Y.M. was also supported by a Heiwa Nakajima Foundation Fellowship and a Stanford Graduate Fellowship. The authors thank Drs. Jessica Xu and March French of Intel Corporation for the nanoindentation measurements and XRR measurements. The authors also thank Dr. William Lanford at U. Albany for the NRA-RBS analysis.

REFERENCES

(1) Dubois, G.; Volksen, W.; Miller, R. D. *Chem. Rev.* **2010**, *110*, 56.
(2) Maex, K.; Baklanov, M. R.; Shamiryan, D.; Iacopi, F.; Brongersma, S. H.; Yanovitskaya, Z. S. *J. Appl. Phys.* **2003**, *93*, 8793.
(3) Lloyd, J. R.; Lane, M. R.; Liu, X. H.; Liniger, E.; Shaw, T. M.; Hu, C. K.; Rosenberg, R. *Microelectron. Reliab.* **2004**, *44*, 1835.
(4) Oliver, M. S.; Dubois, G.; Sherwood, M.; Gage, D. M.; Dauskardt, R. H. *Adv. Funct. Mater.* **2010**, *20*, 2884.
(5) Matsuda, Y.; Rathore, J. S.; Interrante, L. V.; Dauskardt, R. H.; Dubois, G. *Acs Appl. Mater. Interfaces* **2012**, *4*, 2659.
(6) Sanchez, C.; Julian, B.; Belleville, P.; Popall, M. *J. Mater. Chem.* **2005**, *15*, 3559.
(7) Sanchez, C.; Belleville, P.; Popall, M.; Nicole, L. *Chem. Soc. Rev.* **2011**, *40*, 696.
(8) Matsuda, Y.; King, S. W.; Bielefeld, J.; Xu, J.; Dauskardt, R. H. *Acta Mater.* **2012**, *60*, 682.
(9) King, S. W.; Gradner, J. A. *Microelectron. Reliab.* **2009**, *49*, 721.
(10) Stan, G.; King, S. W.; Cook, R. F. *J. Mater. Res.* **2009**, *24*, 2960.
(11) King, S. W.; French, M.; Bielefeld, J.; Lanford, W. A. *J. Non-Cryst. Solids* **2011**, *357*, 2970.
(12) Rouessac, V.; L. Favennec, L.; Rémiat, B.; Jousseaume, V.; Passemard, G.; Durand, J. *Microelectron. Eng.* **2005**, *82*, 333.
(13) Chason, E.; Mayer, T. M. *Crit. Rev. Solid State Mater. Sci.* **1997**, *22*, 1.
(14) Oliver, W. C.; Pharr, G. M. *J. Mater. Res.* **1992**, *7*, 1564.
(15) Zielinski, W.; Huang, H.; Gerberich, W. W. *J. Mater. Res.* **1993**, *8*, 1300.
(16) Kanninen, M. F. *Int. J. Fract.* **1973**, *9*, 83.
(17) Kook, S. Y.; Dauskardt, R. H. *J. Appl. Phys.* **2002**, *91*, 1293.
(18) Gates, S. M.; Neumayer, D. A.; Sherwood, M. H.; Grill, A.; Wang, X.; Sankarapandian, M. *J. Appl. Phys.* **2007**, 101.
(19) Gerbaud, G.; Hediger, S.; Bardet, M.; Favennec, L.; Zenasni, A.; Beynet, J.; Gourhant, O.; Jousseaume, V. *Phys. Chem. Chem. Phys.* **2009**, *11*, 9729.
(20) Gage, D. M.; Stebbins, J. F.; Peng, L. M.; Cui, Z. J.; Al-Bayati, A.; MacWilliams, K. P.; M'Saad, H.; Dauskardt, R. H. *J. Appl. Phys.* **2008**, *104*, 043513.

(21) MacKenzie, K. J. D.; Smith, M. E. *Multinuclear Solid-State NMR of Inorganic Materials*; Pergamon: Oxford, U.K., 2002.
(22) Kudin, A. M.; Rudenko, B. A. *J. Anal. Chem.* **2009**, *64*, 268.
(23) King, S. W.; French, M.; Bielefeld, J.; Lanford, W. A. *J. Non-Cryst. Solids* **2011**, *357*, 2970.
(24) Evans, A. G.; Hutchinson, J. W.; Wei, Y. *Acta Mater.* **1999**, *47*, 4093.
(25) Wei, Y. G.; Hutchinson, J. W. *Int. J. Fract.* **1999**, *95*, 1.
(26) Boolchand, P.; Thorpe, M. E. *Phys. Rev. B* **1994**, *50*, 10366.
(27) Boolchand, P.; Zhang, M.; Goodman, B. *Phys. Rev. B* **1996**, *53*, 11488.
(28) Mauro, J. C. *Am. Ceram. Soc. Bull.* **2011**, *90*, 31.
(29) Phillips, J. C. *J. Non-Cryst. Solids* **1979**, *34*, 153.
(30) Phillips, J. C.; Thorpe, M. F. *Solid State Commun.* **1985**, *53*, 699.
(31) Thorpe, M. F. *J. Non-Cryst. Solids* **1983**, *57*, 355.
(32) King, S. W.; Bielefeld, J.; French, M.; Lanford, W. A. *J. Non-Cryst. Solids* **2011**, *357*, 3602.
(33) Luo, Y.-R., *Comprehensive Handbook of Chemical Bond Energies*; CRC Press: Boca Raton, FL, 2007.
(34) Efstathiadis, H.; Yin, Z.; Smith, F. W. *Phys. Rev. B* **1992**, *46*, 13119.
(35) Matsuda, Y.; King, S. W.; Oliver, M. S.; Dauskardt, R. H. *J. Appl. Phys.* **2013**, *113*, 83521.
(36) Lin, Y.; Xiang, Y.; Tsui, T. Y.; Vlassak, J. *Acta Mater.* **2008**, *56*, 4932.
(37) Iacopi, F.; Travaly, Y.; Eyckens, B.; Waldfried, C.; Abell, T.; Guyer, E. P.; Gage, D. M.; Dauskardt, R. H.; Sajavaara, T.; Houthoofd, K.; Grobet, P.; Jacobs, P.; Maex, K. *J. Appl. Phys.* **2006**, 99.
(38) Robertson, J. *Phys. Rev. Lett.* **1992**, *68*, 220.
(39) Robertson, J. *Diamond Relat. Mater.* **1994**, *3*, 361.
(40) Ferrari, A. C.; Robertson, J. *Phys. Rev. B* **2000**, *61*, 14095.